Bi-level Optimal Operation Model of Mobile Energy Storage System in Coupled Transportation-power Networks

Weiqing Sun, Wei Liu, Jie Zhang, and Kunpeng Tian

***Abstract*—The operation characteristics of energy storage can help the distribution network absorb more renewable energy while improving the safety and economy of the power system. Mobile energy storage systems (MESSs) have a broad application market compared with stationary energy storage systems and electric vehicles due to their flexible mobility and good dispatch ability. However, when urban traffic flows rise, the congested traffic environment will prolong the transit time of MESS, which will ultimately affect the operation state of the power networks and the economic benefits of MESS. This paper proposes a bi-level optimization model for the economic operation of MESS in coupled transportation-power networks, considering road congestion and the operation constraints of the power networks. The upper-level model depicts the daily operation scheme of MESS devised by the distribution network operator (DNO) in order to maximize the total revenue of the system. With fuzzy time windows and fuzzy road congestion indexes, the lower-level model optimizes the route for the transit problem of MESS. Therefore, road congestion that affects the transit time of MESS can be fully incorporated in the optimal operation scheme. Both the IEEE 33-bus distribution network and the 29-node transportation network are used to verify and examine the effectiveness of the proposed model. The simulation results demonstrate that the operation scheme of MESS will avoid the congestion period when considering road congestion. Besides, the transit energy consumption and the impact of the traffic environment on the economic benefits of MESS can be reduced.**

***Index Terms*—Mobile energy storage system, economic dispatch, bi-level optimization model, road congestion, fuzzy constraint.**

NOMENCLATURE

A. Set and Indices

b, b'	Indexes of branches in power networks
g	Index of fossil-energy distributed generations (DGs)
i, j, j'	Indexes of buses in power networks
l	Index of mobile energy storage system (MESS) charging stations
$\hat{l}$	Index of vector dimension
m, n	Indexes of nodes in transportation network
$\mathbb{N}_b$	Set of all branches in power networks
$\mathbb{N}_g$	Set of all fossil-energy DGs
$\mathbb{N}_i$	Set of all buses in power networks
$\mathbb{N}_l$	Set of all MESS charging stations
$\mathbb{N}_m$	Set of all nodes in transportation network
$\mathbb{N}_r$	Set of all renewable energy DGs
$\mathbb{N}_s$	Set of all road sections
$\mathbb{N}_t$	Set of time intervals
r	Index of renewable energy DGs
t, t'	Indexes of time intervals in one day

B. Variables

$\boldsymbol{\xi}$	Vector of error variables
ξ_{it}, ξ_{jt}	Error variables of load on buses i and j during period t
ξ_{rt}	Error variable of renewable energy sources (RESs) during period t
v_g	Binary variable, which equals to 1 if the fossil-energy DG is in "ON" state
$C_{\text{op}}^{\text{DG}}$	Operating cost of fossil-energy DGs
$C_{\text{op}}^{\text{grid}}$	Cost (income) when distribution network operator (DNO) purchases (sells) the electricity from the upper-level power networks
$C_{\text{op}}^{\text{MESS}}$	Operating cost of MESS
$C_{\text{op}}^{\text{RES}}$	Cost of RES purchased by DNO
d	Distance in energy consumption calculation
$d_{m,n,t}$	Driving distance of MESS on road section between nodes m and n during period t
$E_{l,l',t}^{\text{EC}}$	Energy consumption from l to l' during period t
e_m	Departure time at node m

Manuscript received: October 9, 2020; revised: February 6, 2021; accepted: September 10, 2021. Date of CrossCheck: September 10, 2021. Date of online publication: October 29, 2021.

This work was supported in part by the National Natural Science Foundation of China (No. 51777126).

W. Sun, W. Liu (corresponding author), and J. Zhang are with the School of Mechanical Engineering, University of Shanghai for Science and Technology, Shanghai 200093, China (e-mail: sunwq@usst.edu.cn; 15800987750@163.com; zhangjieeeze@163.com).

K. Tian is with the School of Optical-Electrical and Computer Engineering, University of Shanghai for Science and Technology, Shanghai 200093, China (e-mail: 1220837639@qq.com).

DOI: 10.35833/MPCE.2020.000730

f_m, f_n Arrival time at nodes m and n

$h_{m,n,t}$ Time spent on road section between nodes m and n during period t

i^{DNO} Income of DNO

N_t MESS cycles during period t

o_1 Time satisfaction of MESS

o_2, o_2^{norm} Transit time before and after normalization

$o_2^{\max}$, $o_2^{\min}$ The maximum and minimum values by solving o_2

o_3, o_3^{norm} Energy consumptions before and after normalization

o_3^{up}, o_3^{down} Objective functions of the upper- and lower-level models

P_{bt}, Q_{bt} Active and reactive power on branch b during period t

$P_{b't}, Q_{b't}$ Active and reactive power on branch b' during period t

P_{gt}, Q_{gt} Active and reactive power of fossil-energy DG during period t

$P_{lt}^{\mathrm{ch}}, P_{lt}^{\mathrm{dh}}$ Charging and discharging active power for charging station l during period t

$P_t^{\mathrm{grid}}, Q_t^{\mathrm{grid}}$ Active and reactive power from upper-level grid during period t

Q_{lt}^{MESS} Reactive power for charging station l during period t

r_{lt}^{rep} Artificial variable for charging station l during period t

S_t^{SOC} State of charge (SOC) of MESS during period t

S_T^{SOC}, S_0^{SOC} SOCs of MESS at final and initial periods

t^{arr} Arrival time for each MESS transit

$T_{l,l',t}^{\mathrm{transit}}$ Transit time from station l to l' during period t

$T^{\mathrm{st}}, T^{\mathrm{en}}$ Start and end time for each transit

$U_{m,n}$ Binary variable indicating if road section is between nodes m and n

$u_{m,n,t}$ Binary variable indicating if road section is between nodes m and n during period t

v_{it}, v_{jt} Second norms of voltage on buses i and j

v_{it}^0, v_{jt}^0 Voltage on buses i and j without considering error

V^{st}, V^{en} Start and end nodes for each transit

x_{lt} Condition flag for station l during period t

x_{lt}^{ch}, x_{lt}^{dh} Binary variables, which equal to 1 if MESS is charging and discharging for station l during period t

y_{lt} Preparation transit flag for station l during period t

$z_{l,l',t}$ Destination flag from station l to l' during period t

C. Parameters

$\alpha_g, \beta_g, \gamma_g$ Economy coefficients of fossil-energy DG g

λ_1, λ_2, λ_3 Weights of lower-level model functions

ε Probability of constraint failure

ζ Engine module constant

$\eta^{\mathrm{ch}}, \eta^{\mathrm{dh}}$ Charging and discharging efficiencies of MESS

σ Weight of MESS

ψ Speed module constant

ω Weight module constant

Φ_{DG} Linear output range of fossil-energy DG

$\boldsymbol{a}$ Column vector

$\hat{b}$ One-dimensional coefficient vector

B Number of branches in power networks

b_{it}^*, b_{jt}^* Error standard coefficients of load on buses i and j during period t

b_{rt}^* Error standard coefficient of RES on bus i during period t

C^{MESS} Levelized cost of MESS

D Number of buses in power networks

E^{MESS} Rated capacity of MESS

G Number of fossil-energy DGs

$\hat{L}$ Dimension number of $\boldsymbol{a}$

$L_{m,n}$ Road distance between nodes m and n

l^{cost} Labor cost of staff

M Number of MESS charging stations

M^{big} A large number

$N_{\max}$ The maximum number of MESS cycles

P Probability density distribution function satisfied by error variable

P_t^{buy} Purchase price of power for DNO during period t

$P_{\mathrm{RES}}^{\mathrm{buy}}$ Purchase price of RES for DNO

P_{it}, Q_{it} Active and reactive power on bus i during period t

P_{jt}, Q_{jt} Active and reactive power on bus j during period t

P_{it}^0, Q_{it}^0 Predicted active and reactive power on bus i during period t

P_{jt}^0, Q_{jt}^0 Predicted active and reactive power on bus j during period t

P_{rt}, Q_{rt} Active and reactive power of renewable energy DG during period t

P_{rt}^0, Q_{rt}^0 Predicted active and reactive power of renewable energy DG during period t

P_t^{sell} Purchase price of power for users during period t

$P_{\max}^{\mathrm{MESS}}$, $Q_{\max}^{\mathrm{MESS}}$ The maximum active and reactive power of MESS

$P_{\max}^{\mathrm{DG}}$, $P_{\min}^{\mathrm{DG}}$ The maximum and minimum active power of fossil-energy DG

$Q_{\max}^{\mathrm{DG}}$, $Q_{\min}^{\mathrm{DG}}$ The maximum and minimum reactive power of fossil-energy DG

$q_{m,n}$	Road saturation between nodes m and n
$\tilde{q}_{m,n}$	Triangular fuzzy number of road saturation between nodes m and n
$q_{m,n}^{\text{up}}$, $q_{m,n}^{\text{down}}$	Upper- and lower- boundary values of triangular fuzzy number between nodes m and n
R	Number of distributed renewable energy
r^{up}, r^{down}	Climbing rates of load increase and reduction
r_b, x_b	Resistance and reactance on branch b
S^{MESS}	Rated apparent power of MESS
S_b	Apparent power capacity of branch b
S_0^{SOC}	SOC of MESS at initial period
$S_{\max}^{\text{SOC}}$, $S_{\min}^{\text{SOC}}$	The maximum and minimum values of SOC
s	Speed in energy consumption calculation
$s_{m,n,t}$	Moving speed of MESS on road section between nodes m and n during period t
T	Number of simulation periods
T_s	Simulation step size
$v_{\max}$, $v_{\min}$	The maximum and minimum values of second normal voltage

D. Functions

$u(\cdot)$	Membership calculation of fuzzy numbers
$\Pr(\cdot)$	Probability of event occurring
$E^{\text{EC}}(\cdot)$	Energy consumption during transit process

I. Introduction

With the rapid development of wind power and photovoltaics worldwide, a high proportion of renewable energy will become normal in future power systems. The power system with large penetration of renewable energy sources (RESs) will confront the challenges with system planning and operation as well as power supply security and power quality due to the volatility, randomness, and intermittency of RESs [1]. With the technological difficulties and low capital efficiency, promoting RES consumption through a large-scale transformation of the distribution network is clearly not practicable. In this context, the energy storage system (ESS), which has the potential to decouple electricity production and consumption from both time and space dimensions, has emerged as a vital support technology for the future power system with a high penetration of RESs [2].

Demand-side management, energy arbitrage, load smoothing, equipment utilization enhancement, and consumption of RESs can all be accomplished by using ESS [3]. Meanwhile, it can also be applied to enhance system operation stability, adjust frequency, and compensate for load fluctuations [4]. The stationary energy storage system (SESS), which is separated into centralized and distributed ESS based on access manner, is most extensively utilized at this time. Distributed ESS is more favorable in the distribution network with large penetration of RESs due to its ability to swiftly obtain on-site compensation. However, it has greater unit cost than the centralized ESS. To boost scheduling flexibility, the distribution network operator (DNO) must invest more in construction expenditures. The number of electric vehicles (EVs) is growing rapidly, and breakthroughs in vehicle-to-grid (V2G) and grid-to-vehicle (G2V) technologies are achieved. The above conditions make the participation of EVs in power system dispatch a technically feasible option [5]. Although EVs offer good scheduling flexibility, the reliability and controllability of this method will be compromised due to different willingnesses of vehicle owners to participate in the scheduling plan [6].

In view of these, a kind of dedicated large-scale mobile energy storage system (MESS) is gradually emerging. MESS can not only meet the dispatch instructions of DNO in time, but also has the flexibility of EV dispatch. The detailed structure of MESS is given in [7], which is composed of truck body and ESS. The ESS is integrated with a battery cabinet composed of lithium-ion batteries, battery management system (BMS), control circuit, and energy management system (EMS). The benefits that MESS brings to the power system are detailed in Supplementary Material A.

Nowadays, the commercial applications of MESS are becoming more abundant. MESS is currently available at 1000 kW, 5000 kW, and other power levels [8]. In September 2019, it was announced that a 200 MWh MESS power station would be built in the Zhenjiang port power system, China [9]. In November 2019, the MESS was officially put into operation in the Xiong'an New District, China, assisting in the expansion of the distribution network [10]. Furthermore, the battery box project, jointly completed by the French power company and the New Zealand Power Company, was completed in November 2020. The project would provide a large number of MESS units for construction sites and outdoor activities in the Netherlands [11]. In December 2020, the first mobile shared energy storage emergency power base in China (34 MWh in total) was put into operation in Jinhua, China. Through modular, mobile, and shareable energy storage forms, the tasks of optimal power sharing and power quality supervision in the region were realized [12].

With the increasing application of MESS projects, the related theoretical research is getting more and more advanced. Currently, theoretical research on MESS mainly focuses on two aspects.

One is the application of MESS in the restoration of the distribution network after a disaster or the improvement of distribution network resiliency. Aiming at the restoration of the distribution network after natural disasters, [13] coordinates and optimizes various emergency repair resources. In order to solve the problem of rapid recovery after large-area power failure in the distribution system, [14] proposes a joint dispatch scheme of MESS dispatch, microgrid power generation, and distribution network reconstruction. In [15], a two-stage framework is designed to realize the elastic path and scheduling of mobile power resources, including EVs, MESSs, and mobile emergency generations, so as to enhance the distribution network resiliency. A rolling optimization model is proposed in [16], which describes load uncertainty and the status of branches in transportation network or power networks as scenario trees.

The other is the economic scheduling problem of MESS in the distribution network. In [7], MESS is operated with

the objective of maximizing the profitability of the DNO and improving the voltage quality. Given that the MESS investor and DNO are two distinct entities, [17] developes a bi-level day-ahead dispatch model for MESS with voltage control. In [18], the output power and route of the MESS are optimized by establishing linear equations of the distance and time of the movement. As a coupling point between transportation and power networks, the operation scheme of MESS is impacted by the states of both. However, most of the aforementioned literature ignores the influence of the traffic environment on MESS scheduling. With the surge in urban traffic, the road congestion will greatly affect the moving speed and transit time of MESS. Although [18] quantifies the delay time caused by road congestion, it does not consider the effect of road congestion on the moving speed of MESS. Furthermore, the transit model defined in [18] has specific requirements for the transit time matrix. This requirement indicates that the transit time matrix should be obtained from the transportation network that satisfies the consistency condition. If this condition is unsatisfied, then the optimized result is not the optimal operation strategy of MESS.

Based on the above background, this paper establishes a bi-level programming model to develop the economic dispatch of MESS under the coupled transportation-power networks. The general situation of the coupled networks is shown in Fig. B1 of Supplementary Material B. The upper-level model is an economic dispatch model with chance constraints. According to the state of the power networks, the upper-level model formulates the operation plan of MESS and transfers it to the lower level. The lower-level model is a fuzzy route planning model considering road congestion. Based on the state of the transportation network, the route scheme of MESS is updated and returned to the upper level along with the energy consumption. Finally, the bi-level programming model is solved iteratively by the column-and-constraint generation (C&CG) algorithm to obtain the optimal operation scheme of MESS. The main contributions of this paper are as follows.

1) A new transit model of MESS is established. The model does not require whether the transportation network satisfies the consistency condition. For the transportation network that does not satisfy the consistency condition, the upper-level model can still obtain the optimal solution.

2) The uncertainty of road congestion in a time-varying traffic environment is considered. In this paper, the road saturation parameter, which reflects the degree of road congestion, is considered as a fuzzy number and is processed by the expectation value method. On this basis, a route planning scheme with stopping strategy is proposed. With the premise of avoiding road congestion and ensuring time satisfaction, the energy consumption in the transit process is minimized, thus further optimizing the operation economy of MESS.

The rest of this paper is arranged as follows. Firstly, Section II describes the bi-level optimization model for economic dispatch of MESS. Secondly, solution methods are given in Section III. Furthermore, case studies and results are given in Section IV. Finally, Section V provides the conclusion.

II. Bi-level Optimization Model for Economic Dispatch of MESS

With the rapid growth of EVs, electrified transportation with EVs as the core is driving the coupling between the transportation network and power networks, and the deep coupling between them also provides the conditions for the wide application of MESS. In this paper, the main work of MESS is to transit and perform charging/discharging between different charging stations in the transportation network. Before building the model, it is necessary to clarify the meaning of the coupled transportation-power networks. To show the difference, "bus" is used for the power networks, while "node" is used for the transportation network. The specific model of the coupled networks is shown in Supplementary Material C.

A. Upper-level Problem

First and foremost, this paper treats DNO as an MESS investor. Considering the intermittent power generation of RESs and the investment cost of MESS, fossil-energy distributed generations (DGs) are added to the distribution network for auxiliary adjustment such as gas turbines and diesel generations. It should be noted that MESS and fossil-energy DGs are the assets of DNO. RESs are owned by the private company, from whom DNO purchases renewable energy.

1) Objective Function

$$\max o^{\mathrm{up}} = i^{\mathrm{DNO}} - C_{\mathrm{op}}^{\mathrm{grid}} - C_{\mathrm{op}}^{\mathrm{MESS}} - C_{\mathrm{op}}^{\mathrm{DG}} - C_{\mathrm{op}}^{\mathrm{RES}} \tag{1}$$

$$i^{\mathrm{DNO}} = \sum_{t=1}^{T}\sum_{l=1}^{D} P_t^{\mathrm{sell}} P_{it} T_s \tag{2}$$

$$C_{\mathrm{op}}^{\mathrm{grid}} = \sum_{t=1}^{T} P_t^{\mathrm{buy}} P_t^{\mathrm{grid}} T_s \tag{3}$$

$$C_{\mathrm{op}}^{\mathrm{MESS}} = C^{\mathrm{MESS}} \sum_{t=1}^{T}\sum_{l=1}^{M} \eta^{\mathrm{ch}} P_{lt}^{\mathrm{ch}} T_s + l^{\mathrm{cost}} \tag{4}$$

$$C_{\mathrm{op}}^{\mathrm{DG}} = \sum_{t=1}^{T}\sum_{g=1}^{G}\left[\alpha_g \left(P_{gt} T_s\right)^2 + \beta_g P_{gt} T_s + \gamma_g\right] \tag{5}$$

$$C_{\mathrm{op}}^{\mathrm{RES}} = \sum_{t=1}^{T}\sum_{r=1}^{R} P_{\mathrm{RES}}^{\mathrm{buy}} P_{rt} T_s \tag{6}$$

The objective function is to maximize the profit of DNO, as shown in (1).

2) Power Flow Constraints

This paper adopts the linear dist-flow branch power flow model [19] based on radial distribution networks, which is widely used in the optimal operation of distribution network [20].

$$P_{bt} = \sum_{\forall b' \in \mathbb{N}_b, b' = (j,j'), j' \neq i, j' \in \mathbb{N}_i} \left(P_{b't} + P_{jt} + P_{lt}^{\mathrm{ch}} + P_{lt}^{\mathrm{dh}} - P_{gt} - P_{rt}\right)$$
$$\forall b \in \mathbb{N}_b, b = (i,j), i,j \in \mathbb{N}_i, t \in \mathbb{N}_t, l \in \mathbb{N}_l, g \in \mathbb{N}_g, r \in \mathbb{N}_r \tag{7}$$

$$Q_{bt} = \sum_{\forall b' \in \mathbb{N}_b, b' = (j,j'), j' \neq i, j' \in \mathbb{N}_i} \left(Q_{b't} + Q_{jt} + Q_{lt}^{\mathrm{MESS}} - Q_{gt} - Q_{rt}\right) \tag{8}$$

$$v_{jt} = v_{it} - 2\left(r_b P_{bt} + x_b Q_{bt}\right) \tag{9}$$

$$v_{\min} \le v_{it} \le v_{\max} \tag{10}$$

In (7)-(10), the square of voltage on buses i or j is repre-

sented by a single variable v_{it} or v_{jt} to ensure the linearity of the equation. Specific linear dist-flow power flow equations are given in Supplementary Material C.

3) Operation Constraints of MESS

The operation constraints of MESS consist of two parts: ESS operation model and transit model. The ESS operation model limits the state of charge (SOC) [21], the number of cycles, and the charging/discharging power [22].

$$\left(P_{lt}^{\mathrm{ch}}+P_{lt}^{\mathrm{dh}}\right)^2+\left(Q_{lt}^{\mathrm{MESS}}\right)^2\le\left(S^{\mathrm{MESS}}\right)^2 \tag{11}$$

$$0\le P_{lt}^{\mathrm{ch}}\le P_{\max}^{\mathrm{MESS}}x_{lt}^{\mathrm{ch}} \tag{12}$$

$$-P_{\max}^{\mathrm{MESS}}x_{lt}^{\mathrm{dh}}\le P_{lt}^{\mathrm{dh}}\le 0 \tag{13}$$

$$x_{lt}^{\mathrm{ch}}+x_{lt}^{\mathrm{dh}}\le x_{lt} \tag{14}$$

$$-Q_{\max}^{\mathrm{MESS}}x_{lt}\le Q_{lt}^{\mathrm{MESS}}\le Q_{\max}^{\mathrm{MESS}}x_{lt} \tag{15}$$

$$S_{\min}^{\mathrm{SOC}}\le S_t^{\mathrm{SOC}}\le S_{\max}^{\mathrm{SOC}} \tag{16}$$

$$S_T^{\mathrm{SOC}}=S_0^{\mathrm{SOC}} \tag{17}$$

$$N_t\le N_{\max} \tag{18}$$

$$S_{t+1}^{\mathrm{SOC}}=S_t^{\mathrm{SOC}}+\frac{T_s}{E^{\mathrm{MESS}}}\left(\eta^{\mathrm{ch}}P_{lt}^{\mathrm{ch}}+\eta^{\mathrm{dh}}P_{lt}^{\mathrm{dh}}-\sum_{t=1}^{T}\sum_{l=1}^{2M}\sum_{l'=1}^{2M}z_{l',l,t}E_{l',l,t}^{\mathrm{EC}}\right) \tag{19}$$

$$N_{t+1}=N_t+\frac{T_s}{2E^{\mathrm{MESS}}}\left(\eta_{\mathrm{ch}}P_{lt}^{\mathrm{ch}}-\eta_{\mathrm{dh}}P_{lt}^{\mathrm{dh}}+\sum_{t=1}^{T}\sum_{l=1}^{2M}\sum_{l'=1}^{2M}z_{l',l,t}E_{l',l,t}^{\mathrm{EC}}\right) \tag{20}$$

Equation (17) guarantees the MESS cycles. In [7], the equation for calculating the number of MESS cycles is given. But unlike the fuel-consuming truck in [7], this paper assumes that the truck consumes the electricity. Therefore, an item $\sum_{t=1}^{T}\sum_{l=1}^{2M}\sum_{l'=1}^{2M}z_{l',l,t}E_{l',l,t}^{\mathrm{EC}}$ is added, which is used to calculate the energy consumption of MESS during its transit. For the same reason, this term is added to both (19) and (20). Note that as a parameter of the upper-level model, $E_{l',l,t}^{\mathrm{EC}}$ is obtained by optimizing the lower-level model.

The transit models of [7] and [17] are nonlinear models, which affect the solution efficiency. In order to eliminate the nonlinearity, [18] builds a linear transit model for MESS based on [23]. However, the linear model requires that the transit time matrix must be obtained through a transportation network that satisfies the consistency condition [24].

In short, a transportation network satisfying the consistency condition means that vehicles that depart earlier would arrive at their destinations earlier than those that depart later. Since the linear transit model has high data requirements for the transit time matrix, it cannot solve the scenarios where the transportation network does not satisfy the consistency condition, e.g., when road congestion or traffic accident occurs. For this reason, a novel transit model is developed in this paper, which does not have high data requirements for the transit time matrix.

$$y_{lt}=x_{l(t+1)}-x_{lt} \tag{21}$$

$$\begin{cases} z_{l,l',t}=round\left(\dfrac{x_{lt}+x_{l'\left(t+T_{l,l',t}^{\mathrm{transit}}+1\right)}}{2.1}\right) & \sum_{l=1}^{M}\sum_{t=t'}^{t'+T_{l,l',t}^{\mathrm{transit}}}x_{lt}=0 \\ z_{l,l',t}=0 & \sum_{l=1}^{M}\sum_{t=t'}^{t'+T_{l,l',t}^{\mathrm{transit}}}x_{lt}\ne 0 \end{cases} \tag{22}$$

$$x_{l(t+1)}=round\left(\frac{\sum_{l'=1}^{M}\left(1-z_{l,l',t}\right)}{M}\right)y_{lt}+round\left(\frac{x_{lt}+x_{l(t+1)}}{2.1}\right) \tag{23}$$

$$\sum_{l=1}^{M}x_{lt}\le 1\ \sum_{l=1}^{M}x_{l1}=1\ \sum_{l=1}^{M}x_{lT}=1\quad\forall t\in\mathbb{N}_t \tag{24}$$

$$\sum_{l=1}^{M}\sum_{l'=1}^{M}z_{l,l',t}\le 1\quad\forall t\in\mathbb{N}_t \tag{25}$$

Detailed explanations of (21)-(25) are given in Supplementary Material D.

4) Operation Constraints of DG

In this paper, DGs of two energy types are considered. One is in the form of renewable energy, and the other is in the form of fossil energy. The output of fossil-energy DGs is the only factor that is constrained. To ensure that the equation is a convex one, the output power of fossil-energy DGs is constrained to be linear [22]. The specific linear range equation can be found in Fig. B2 of Supplementary Material B.

$$\left(P_{gt},Q_{gt}\right)\in\Phi_{\mathrm{DG}} \tag{26}$$

$$v_g P_{\min}^{\mathrm{DG}}\le P_{gt}\le v_g P_{\max}^{\mathrm{DG}} \tag{27}$$

$$v_g Q_{\min}^{\mathrm{DG}}\le Q_{gt}\le v_g Q_{\max}^{\mathrm{DG}} \tag{28}$$

$$P_{gt}-r^{\mathrm{up}}\le P_{g(t+1)}\le P_{gt}+r^{\mathrm{down}} \tag{29}$$

5) Chance Constraints

Due to the uncertainty of RESs and load forecasting, the chance constraint method is used to deal with the randomness of both. It is assumed that the actual power of RESs and load can be divided into two parts: predicted value and error value. At the same time, the power factors of RESs and load are assumed to be constant.

$$P_{rt}=P_{rt}^0+b_{rt}^*\xi_{rt} \tag{30}$$

$$P_{it}=P_{it}^0+b_{it}^*\xi_{it} \tag{31}$$

$$Q_{rt}=P_{rt}Q_{rt}^0/P_{rt}^0 \tag{32}$$

$$Q_{it}=P_{it}Q_{it}^0/P_{it}^0 \tag{33}$$

Affected by the randomness of RESs and load, voltage and current may exceed the limits. Therefore, the corresponding chance constraints are constructed to describe this phenomenon. The chance constraints of branch power flow are shown in Supplementary Material E.

$$\Pr\left(v_{it}\le v_{\max}\right)\ge 1-\varepsilon \tag{34}$$

$$\Pr\left(v_{it}\ge v_{\min}\right)\ge 1-\varepsilon \tag{35}$$

B. Lower-level Problem

After the lower-level model gets the operation scheme of

MESS from the upper-level model, it needs to re-route each transit process of MESS to reduce energy consumption as much as possible. Therefore, the lower-level model is essentially a time-dependent route planning model.

To quantify the energy consumption of MESS during road congestion, the energy consumption model given in [25] is adopted. As shown in (36), energy consumption is determined by three factors: speed s, transit distance d, and weight σ.

$$E^{\mathrm{EC}}(d,s,\sigma)=\omega\sigma d+\zeta\frac{d}{s}+\psi d s^2 \tag{36}$$

Since the road congestion is often accompanied by frequent acceleration and deceleration of vehicles, the change in speed will affect the energy consumption. To visually depict this variation, Fig. 1 shows the the relationship between energy consumption and speed, where V_a and V_b are two different reference speeds.

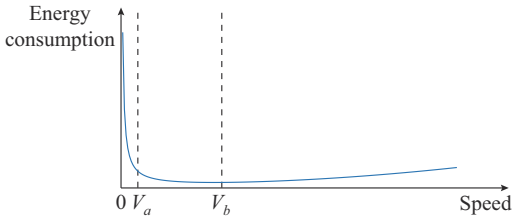

Fig. 1. Relationship between energy consumption and speed.

It is clear that either too high or too low speed leads to high energy consumption, especially at low speeds. In order to ensure that MESS can keep the driving speed with low energy consumption during the transit, a route planning scheme that includes a stopping strategy is proposed. In Fig. 2, the speeds of road section between nodes m and n at different periods are given.

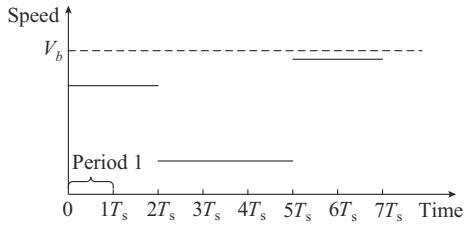

Fig. 2. Time-dependent speed profile.

The transit comparison of MESS on road section between nodes m and n with and without stopping strategy is given in Fig. 3.

It can be found that the route planning, including the stopping strategy, keeps the MESS moving at a good speed. To balance the relationship between the transit time and energy consumption, the arrival time of MESS t^{arr} is extended into a fuzzy time window and the membership function of fuzzy numbers is used to describe the time satisfaction of arriving at the charging station. By setting three objective functions in the lower-level model, (37) denotes the time satisfaction, (38) denotes the transit time, and (39) denotes the energy consumption, and the energy consumption is minimized while ensuring time satisfaction.

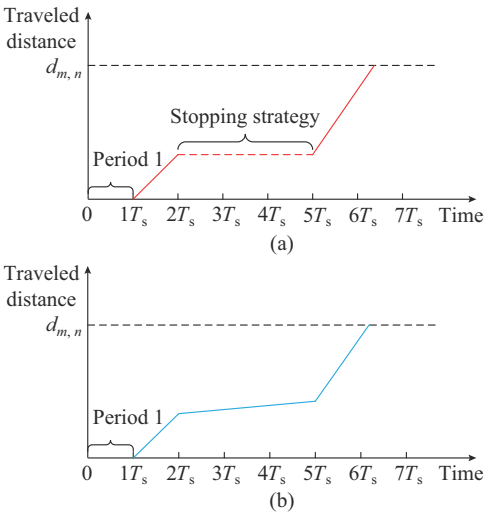

Fig. 3. Transit comparison of MESS with and without stopping strategy. (a) With stopping strategy. (b) Without stopping strategy.

$$\min o_1=-\sigma\left(t^{\mathrm{arr}}\right) \tag{37}$$

$$\min o_2=t^{\mathrm{arr}}-T^{\mathrm{st}} \tag{38}$$

$$\min o_3=E^{\mathrm{EC}}\left(d_{m,n,t},s_{m,n,t},\sigma\right)=\sum_{(m,n)\in\mathbb{N}_m}\sum_{t\in\mathbb{N}_t}\left(\omega\sigma d_{m,n,t}+\zeta\frac{d_{m,n,t}}{s_{m,n,t}}+\psi d_{m,n,t}s_{m,n,t}^2\right) \tag{39}$$

In order to obtain the speed parameter $s_{m,n,t}$, it is necessary to quantitatively evaluate the road congestion condition of each road section at each time period. Since there is no unified international standard for the quantitative analysis of road congestion, this paper will adopt the Evaluation Index System of Urban Traffic Management issued by the Ministry of Public Security of China [26]. The evaluation of road congestion includes various quantitative indexes such as road section saturation, traffic flow density, queue length, and congestion duration [26]. To simplify the evaluation process, road section saturation $q_{m,n}$ is used as a single factor index to evaluate road congestion. The index is the ratio of traffic flow on a road section to the capacity of that road section. The traffic flow of a road section can be predicted based on historical traffic flow data by a Bayesian time-series model [27], online support vector regression [28], neural network model [29], or other methods [30]. When the index exceeds the set threshold, the road section is judged to be in road congestion. The corresponding congestion levels are derived based on specific values, and the quantitative relationships are shown in Table BI of Supplementary Material B. Considering the influence of various uncertainties in the transportation network, the predicted road saturation is described as a fuzzy number to reflect its volatility. On the basis of the fuzzy programming method proposed in [31], the arrival time of each transit and road section saturation are regarded as a trapezoidal fuzzy number and a triangular fuzzy number, respectively. The specific meanings are explained in Supplementary Material F.

The route planning constraints are:

$$\sum_{\forall(m,n)\in\mathbb{N}_m} U_{m,n} - \sum_{\forall(m,n)\in\mathbb{N}_m} U_{n,m} = \begin{cases} 1 & m = V^{\mathrm{st}} \\ 0 & m \neq V^{\mathrm{st}}, m \neq V^{\mathrm{en}} \\ -1 & m = V^{\mathrm{en}} \end{cases} \tag{40}$$

$$0 \le d_{m,n,t} \le L_{m,n} u_{m,n,t} \quad \forall (m,n) \in \mathbb{N}_m, t \in \mathbb{N}_t \tag{41}$$

$$u_{m,n,t} \le U_{m,n} \le \sum_{t\in\mathbb{N}_t} u_{m,n,t} \quad \forall (m,n) \in \mathbb{N}_m, t \in \mathbb{N}_t \tag{42}$$

$$\sum_{t\in\mathbb{N}_t} d_{m,n,t} = U_{m,n} L_{m,n} \quad \forall (m,n) \in \mathbb{N}_m \tag{43}$$

$$h_{m,n,t} = \frac{60 d_{m,n,t}}{s_{m,n,t}} \quad \forall (m,n) \in \mathbb{N}_m, t \in \mathbb{N}_t \tag{44}$$

$$\sum_{\forall(m,n)\in\mathbb{N}_m} h_{m,n,t} \le 60 T_s \quad \forall t \in \mathbb{N}_t \tag{45}$$

$$\begin{cases} e_m \le 60 T_s t - h_{m,n,t} + 60 T_s T\left(1 - u_{m,n,t}\right) & \forall (m,n) \in \mathbb{N}_m, t \in \mathbb{N}_t \\ f_n \le 60 T_s (t-1) + h_{m,n,t} - 60 T_s T\left(1 - u_{m,n,t}\right) & \forall (m,n) \in \mathbb{N}_m, t \in \mathbb{N}_t \\ f_n \ge e_m + \sum_{t\in\mathbb{N}_t} h_{m,n,t} - 60 T_s T\left(1 - U_{m,n}\right) & \forall (m,n) \in \mathbb{N}_m, t \in \mathbb{N}_t \end{cases} \tag{46}$$

$$0 \le f_m \le e_m \quad \forall m \in \mathbb{N}_m \tag{47}$$

$$t^{\mathrm{arr}} = f_m \quad m = V^{\mathrm{en}} \tag{48}$$

$$h_{m,n,t} \ge 0 \quad \forall (m,n) \in \mathbb{N}_m, t \in \mathbb{N}_t \tag{49}$$

$$E^{\mathrm{EC}}\left(d_{m,n,t}, s_{m,n,t}, \sigma\right) \le \left(S^{\mathrm{SOC}}_{T^{\mathrm{st}}} - S^{\mathrm{SOC}}_{T^{\mathrm{en}}}\right) E^{\mathrm{MESS}} \tag{50}$$

The specific meanings of the above constraints are explained in the Supplementary Material G.

III. Solution Methods

Through the above modeling, it can be found that the upper-level model is a stochastic programming with chance constraints, and the lower-level model is a multi-objective programming with fuzzy parameters. To facilitate the problem solving, the models will be transformed to deterministic forms.

Referring to the methods in [32] and [33], the approximation of the chance constraint for the upper model can be calculated. When the random variable obeys a symmetrical distribution or even a Gaussian distribution, the chance constraint (51) can be rewritten as (52).

$$\Pr_{\xi\sim P}\left\{\boldsymbol{a}^{\mathrm{T}}\boldsymbol{\xi} + \hat{b} > 0\right\} \le \varepsilon \tag{51}$$

$$\hat{b} + \sqrt{2\ln\left(\frac{1}{\varepsilon}\right)\sum_{l=1}^{\hat{L}} a_l^2} \le 0 \tag{52}$$

Specific derivation process of the approximation processing can be found in Supplementary Material E.

Thus, the chance constraints in the upper-level model can be transformed to deterministic forms. It is assumed that the errors in RES output and load prediction are symmetrically distributed and independent of each other. According to (7)-(8) and (30)-(33), a linear equation between the voltage and the above error variables can be derived.

$$\begin{aligned} v_{jt} = v_{jt}^0 - 2\Big\{ & r_b\left(b_{jt}^* \xi_{jt} - b_{rt}^* \xi_{rt}\right) + \\ & x_b\left[b_{jt}^* \xi_{jt} Q_{jt}^0 / P_{jt}^0 - b_{rt}^* \xi_{rt} Q_{rt}^0 / P_{rt}^0\right]\Big\} = \\ & v_{jt}^0 - 2\left[\left(r_b b_{jt}^* + x_b b_{jt}^* Q_{jt}^0 / P_{jt}^0\right)\xi_{jt} - \left(r_b b_{rt}^* + x_b b_{rt}^* Q_{rt}^0 / P_{rt}^0\right)\xi_{rt}\right] \end{aligned} \tag{53}$$

Substitute (53) into the chance constraint (52), and then transform it into the following deterministic equations.

$$v_{jt}^0 - v_{\max} + \sqrt{2\ln(1/\varepsilon)\left\{\left[-2\left(r_b b_{jt}^* + x_b b_{jt}^* Q_{jt}^0 / P_{jt}^0\right)\right]^2 + \left[2\left(r_b b_{rt}^* + x_b b_{rt}^* Q_{rt}^0 / P_{rt}^0\right)\right]^2\right\}} \le 0 \tag{54}$$

$$-v_{jt}^0 + v_{\min} + \sqrt{2\ln(1/\varepsilon)\left\{\left[2\left(r_b b_{jt}^* + x_b b_{jt}^* Q_{jt}^0 / P_{jt}^0\right)\right]^2 + \left[-2\left(r_b b_{rt}^* + x_b b_{rt}^* Q_{rt}^0 / P_{rt}^0\right)\right]^2\right\}} \le 0 \tag{55}$$

Similarly, the chance constraints of branch power flow can also be transformed deterministically. See Supplementary Material E for specific steps.

After the deterministic conversion, the error variable is no longer included, so v_{jt}^0 can be replaced by v_{jt}. Obviously, the transformed constraints are the contraction of the original constraints, which reflect the robustness of the chance constraints.

Since the former part of (23) has a value of 1 or 0, it can be considered as a binary variable. Therefore, (23) contains the product of two variables and is a nonconvex constraint. To eliminate the nonconvexity, (23) is linearized by adding the artificial variable r_{lt}^{rep} and using the big M M^{big} method.

$$0 \le -r_{lt}^{\mathrm{rep}} + y_{lt} \le M^{\mathrm{big}}\left\{1 - round\left(\sum_{l=1}^{M}\sum_{l'=1}^{M}\left(1 - z_{l,l',t}\right) \Big/ \left(2M-1\right)\right)\right\} \tag{56}$$

$$-M^{\mathrm{big}} \cdot round\left(\sum_{l=1}^{M}\sum_{l'=1}^{M}\left(1 - z_{l,l',t}\right) \Big/ \left(2M-1\right)\right) \le r_{lt}^{\mathrm{rep}} \tag{57}$$

$$r_{lt}^{\mathrm{rep}} \le M^{\mathrm{big}} \cdot round\left(\sum_{l=1}^{M}\sum_{l'=1}^{M}\left(1 - z_{l,l',t}\right) \Big/ \left(2M-1\right)\right) \tag{58}$$

By adding r_{lt}^{rep} in (23), we can obtain:

$$x_{l(t+1)} = r_{lt}^{\mathrm{rep}} + round\left(\frac{x_{lt} + x_{l(t+1)}}{2.1}\right) \tag{59}$$

For the lower-level model, it is necessary to deal with the fuzzy number $\tilde{q}_{m,n}$ and the multi-objective function. Firstly, the expected interval and the expected value of the triangular fuzzy number are presented through the membership function [34]. The details are as follows.

$$u\left(\tilde{q}_{m,n}\right)=\begin{cases}0 & \forall \tilde{q}_{m,n}\in\left[0,q_{m,n}^{\mathrm{d}}\right] \text{ or } \tilde{q}_{m,n}\in\left[q_{m,n}^{\mathrm{u}},1\right]\\ \dfrac{\tilde{q}_{m,n}-q_{m,n}^{\mathrm{down}}}{q_{m,n}-q_{m,n}^{\mathrm{up}}} & \forall \tilde{q}_{m,n}\in\left(q_{m,n}^{\mathrm{d}},q_{m,n}\right)\\ 1 & \tilde{q}_{m,n}=q_{m,n}\\ \dfrac{q_{m,n}^{\mathrm{up}}-\tilde{q}_{m,n}}{q_{m,n}^{\mathrm{up}}-q_{m,n}} & \forall \tilde{q}_{m,n}\in\left(q_{m,n},q_{m,n}^{\mathrm{up}}\right)\end{cases} \tag{60}$$

The expected interval is:

$$\tilde{q}_{m,n}=\begin{cases}\dfrac{1}{2}\left(q_{m,n}^{\mathrm{down}}+q_{m,n}\right)\\ \dfrac{1}{2}\left(q_{m,n}^{\mathrm{up}}+q_{m,n}\right)\end{cases} \tag{61}$$

The expected value is:

$$\tilde{q}_{m,n}=\frac{1}{4}\left(q_{m,n}^{\mathrm{down}}+2q_{m,n}+q_{m,n}^{\mathrm{up}}\right) \tag{62}$$

The fuzzy number of road section saturation $\tilde{q}_{m,n}$ can be transformed by the expected value of $\tilde{q}_{m,n}$, and then the speed of MESS in the corresponding road section can be obtained according to the Table BI of Supplementary Material B.

Secondly, the efficiency coefficient method is used to convert multiple objectives into a single objective, i.e., each objective function is normalized. Since o_1 is in the range of [0,1], only o_2 and o_3 are treated.

$$o_2^{\mathrm{norm}}=\frac{o_2-o_2^{\mathrm{min}}}{o_2^{\mathrm{max}}-o_2^{\mathrm{min}}} \tag{63}$$

$$o_3^{\mathrm{norm}}=\frac{o_3-o_3^{\mathrm{min}}}{o_3^{\mathrm{max}}-o_3^{\mathrm{min}}} \tag{64}$$

$$o^{\mathrm{down}}=\lambda_1 o_1+\lambda_2 o_2^{\mathrm{norm}}+\lambda_3 o_3^{\mathrm{norm}} \tag{65}$$

In the above equations, $0\le\lambda_1\le 1$, $0\le\lambda_2\le 1-\lambda_1$, and $0\le\lambda_3\le 1$ ($\lambda_3=1-\lambda_1-\lambda_2$) are used to control the ratio of the three functions.

Finally, the upper-level problem is transformed into a mixed-integer second-order cone programming problem, and the lower-level problem is transformed into a mixed-integer programming problem. The bi-level programming problem can be summarized as:

$$\begin{cases}\max\ o^{\mathrm{up}}=i^{\mathrm{DNO}}-C_{\mathrm{op}}^{\mathrm{grid}}-C_{\mathrm{op}}^{\mathrm{MESS}}-C_{\mathrm{op}}^{\mathrm{DG}}-C_{\mathrm{op}}^{\mathrm{RES}}\\ \text{s.t. (7)-(9), (11)-(22), (24)-(29), (54)-(59)}\\ \min\ o^{\mathrm{down}}=\lambda_1 o_1+\lambda_2 o_2^{\mathrm{norm}}+\lambda_3 o_3^{\mathrm{norm}}\\ \text{s.t. (40)-(50)}\end{cases} \tag{66}$$

Given that the lower-level model contains binary variables, it is impossible to convert the bi-level model into a single-level model through strong duality theory or Karush-Kuhn-Tucker (KKT) optimality conditions. Hence, according to the methods in [35] and [36], the bi-level model is decomposed into the master problem and subproblem, and the C&CG algorithm is used to solve the problem. The specific solution procedure is shown in Supplementary Material H.

IV. Case Studies and Results

A. Test Networks and Case Study Conditions

The coupled transportation-power networks consisting of an IEEE 33-bus distribution network and a 29-node transportation network [37] are chosen as the test network to verify the validity of the above model. The network topologies are shown in Figs. B3 and B4 of Supplementary Material B.

The detailed information about the coupled networks is as follows. The rated capacity and rated voltage of the power networks are 10 MVA and 12.66 kV, respectively; the power networks has 33 buses and 32 branches; and the transportation network has 29 nodes and 49 roads. The mapping relationship between power networks buses and transportation network nodes is shown in Table BII of Supplementary Material B. The mapping relationship between road sections and nodes in the transportation network is shown in Table BIII of Supplementary Material B.

According to the load characteristics, the areas are divided into residential, suburban, industrial, and commercial areas. And the load curves, wind power output curves, and photovoltaic output curves for each zone are generated by the methods in [38]-[40], as shown in Figs. B5 and B6 of Supplementary Material B. Since the planning of charging stations and the configuration of MESS capacity are not part of the discussion in this paper, the method in [41] is used to solve these problems. The results of charging station planning show a total of three charging stations: charging station 1 located on bus 2 (node 2), charging station 2 located on bus 17 (node 14), and the charging station 3 located on bus 33 (node 27). The capacity configuration of MESS results in 2.5 MW/5 MWh. Since there are few single MESSs with such a large capacity on the electricity market, the same capacity is achieved by configuring five MESSs all with a rated capacity of 500 kW/1 MWh. The five MESSs are considered as a whole during the development of the dispatch plan.

Regarding the setting of the chance constraint parameter in the upper-level model, the probability of not satisfying the inequality constraint is set to be 0.05, i.e., $\varepsilon=0.05$. The sample values of the forecasting error of load and the output error of RESs are randomly generated from two normal distributions $N(0,0.06)$. These two normal distributions are independent of each other and both take values in the range of [−1, 1]. In addition, the electricity price is shown in Fig. 4.

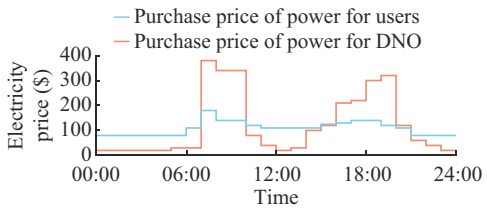

Fig. 4. Electricity price.

The planning results of the lower-level model include the energy consumption of a single MESS in a single transit, but the final energy consumption is generated by multiple MESSs in multiple transits. Therefore, the lower-level model needs to

be cycled through the optimization several times to generate the final energy consumption. In addition, the saturation of each road section at each time period based on the predicted traffic flow is shown in Fig. B7 of Supplementary Material B.

The optimization models are implemented in MATLAB with the YALMIP toolbox [42], on a computer with an Intel i7-10710U processor and 16 GB RAM of memory. To solve the involved mixed-integer programming problems, GUROBI 9.0 is used [43]. The convergence gap φ is set to be 0.5%. More basic data is shown in Table BIV of Supplementary Material B.

B. Case Study Results

Based on the established mathematical model and the designed solving process, the optimal scheduling scheme can be solved. The iteration and computation time are shown in Table I. In addition, the number of subproblems to be solved in each iteration depends on that of MESS transits. Based on the solution results, the analysis is carried out in three aspects: economy, energy consumption in the transit process, and comparison of transit models.

TABLE I
ITERATION AND COMPUTATION TIME

Iteration	Total calculation time (s)	Single calculation time of master problem (s)	Single calculation time of subproblem (s)
3	2389.76	390.28	68.52

1) Economic Analysis

Firstly, the index parameters of the original system and the system with MESS are analyzed from the economic point of view. According to the data in Table II, it can be seen that the daily profit of the system with MESS increases from \$6355.1 to \$7226.5. And the maximum/minimum/average voltage and voltage standard deviation show the improvement of voltage quality brought by MESS. According to the voltage comparison in Fig. 5, it is clear that the addition of MESS has maintained the system voltage within the safe fluctuation range at all times.

TABLE II
INDEX PARAMETERS OF ORIGINAL SYSTEM AND SYSTEM WITH MESS

System	Profit (\$)	The maximum voltage (kV)	The minimum voltage (kV)	Average voltage (kV)	Voltage standard deviation
Original system	6355.1	13.6960	12.0064	12.7617	0.2901
System with MESS	7226.5	13.2879	12.0320	12.6617	0.2629

Figure 6 shows that MESS transits three times a day. MESS transits from charging station 3 to charging station 2 at 03:00, from charging station 2 to charging station 3 at 09:00, and from charging station 3 to charging station 1 at 19:40. It is not difficult to find that the departure time of MESS tries to avoid the morning peak (07:30-09:00) and the evening peak (17:30-18:30), which are common periods of road congestion.

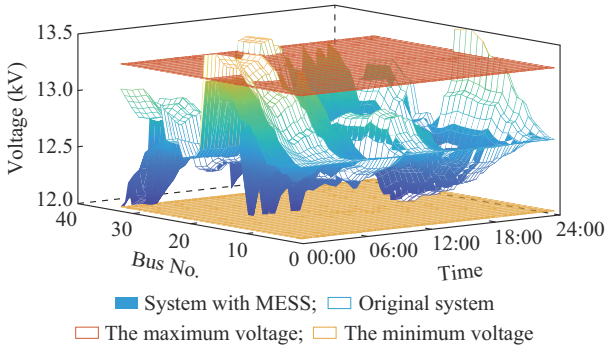

Fig. 5. Voltage comparison between original system and system with MESS.

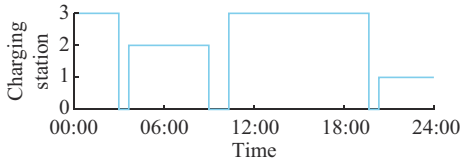

Fig. 6. Diagram of MESS transit with stopping strategy.

The charging or discharging of MESS is not only driven by the electricity price, but also by the net load of the system. The net load of the system can be understood by observing the output of fossil-energy DGs.

For example, the output of fossil-energy DGs is generally at its peak during periods with large values of net load. And the output of fossil-energy DGs is generally at a trough during periods with small values of net load. As shown in Fig. 7, the output of fossil-energy DGs is low between 00:00 and 06:00, indicating that the value of net load is small during this period. During this period, the difference between the electricity price sold P^{sell} and the electricity price bought P^{buy} is larger. The above phenomenon suggests that MESS is charged between 00:00 and 06:00 to ensure the economy while mitigating voltage fluctuations in the system. In contrast, between 07:00 and 08:00, the value of net load is higher and the difference between P^{buy} and P^{sell} is larger. Therefore, MESS is discharged between 07:00 and 08:00, which not only makes high profits but also raises the system voltage. The reasons for charging or discharging MESS during the rest of the time period are consistent with the previous narrative and will not be repeated. The operational status of MESS with stopping strategy is shown in Fig. 8. In addition, it can be observed from Fig. 9 that the MESS performs energy arbitrage while also providing reactive power support to the power system.

2) Analysis of Transit Energy Consumption

To get a clear picture of the impact of the stopping strategy, specific path of each transit process, total energy consumption, and transit time are given in Tables III and IV. It should be noted that since the simulation step T_s of the upper-level model is 1/3 hour (20 min), and the difference between the arrival time and departure time should be an integer multiple of T_s. The comparison of the parameters in Table III and Table IV shows that the energy consumption with the stopping strategy can be reduced by 191.9870 kWh. As a

commercial use of MESSs, the value of the reduced energy consumption will grow.

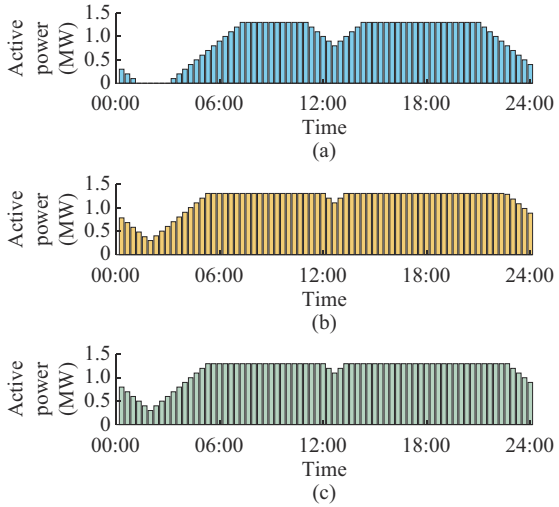

Fig. 7. Active power of fossil-energy DGs. (a) DG 1. (b) DG 2. (c) DG 3.

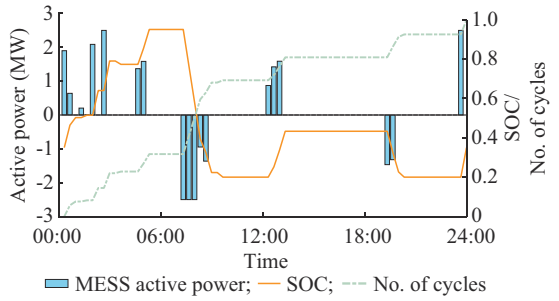

Fig. 8. Operational status of MESS with stopping strategy.

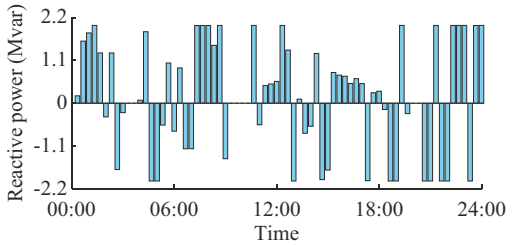

Fig. 9. MESS reactive power with stopping strategy.

TABLE III
TRANSIT PROCESS WITH STOPPING STRATEGY

Transit No.	Transit route (node No.)	Energy consumption (kWh)	Departure time	Arrival time	Transit time (min)
1	14→24→23→22→27	16.9965 × 5	03:00	03:40	21.77
2	14→21→25→26→27	23.3546 × 5	09:00	10:20	66.40
3	2→1→4→7→20→22→27	26.5428 × 5	19:40	20:20	31.95

The process of transit No. 2 is used as an example to further observe when MESS adopts a stopping strategy to avoid road congestion. Tables V and VI show the transit distances of MESS for each road section during the process of transit No. 2 with stopping strategy and without non-stopping strategy, respectively. It is clear that between 9:00 and 10:00, road congestion will occur in the road sections near node 27, i.e., charging station 3. With the stopping strategy, MESS will not continue to move when MESS is transferred to node 25. MESS will continue to move to node 27 only after the road congestion has been alleviated. However, under the non-stopping strategy, MESS will continue to move to node 27 at a slow speed.

TABLE IV
TRANSIT PROCESS WITHOUT STOPPING STRATEGY

Transit No.	Transit route (node No.)	Energy consumption (kWh)	Departure time	Arrival time	Transit time (min)
1	14→24→23→26→27	17.9510 × 5	03:00	03:40	21.41
2	14→21→25→24→23→22→27	49.8512 × 5	09:00	10:00	54.50
3	2→1→4→7→20→22→27	37.4891 × 5	19:40	20:20	27.81

TABLE V
TRANSIT DISTANCE OF ROAD SECTION WITH STOPPING STRATEGY

Road section	Transit distance of different time (km)			
	09:00-09:20	09:20-09:40	09:40-10:00	10:00-10:20
14→21	8.70			
21→25	3.18			
25→26				2.4
26→27				4.8

TABLE VI
ROAD SECTION TRANSIT DISTANCE WITHOUT STOPPING STRATEGY

Road section	Transit distance of different time (km)			
	09:00-09:20	09:20-09:40	09:40-10:00	10:00-10:20
14→21	8.7000			
21→25	3.1800			
25→24	4.9500			
24→23	3.6000			
23→22	3.3000			
22→27	0.1249	1.6667	1.2085	

The traversal method is used to determine the weights of each objective function in the lower-level model, and the traversal step is 0.01. Taking the process of transit No. 2 as an example, 300 optimal solutions are obtained by traversing the weights of the three objective functions. These 300 optimal solutions can be categorized into three types, as shown in Table VII. It is not difficult to find that in the first type of solution, i.e., type I, λ_1 and λ_2 are larger, resulting in higher energy consumption o_3. However, the third type of solution, i.e., type III, has a higher λ_3, resulting in a longer transit time o_2. In summary, the type II solution has the best weight and will be used as the final weight, i.e., $\lambda_1 = 0.3$, $\lambda_2 = 0.3$, and $\lambda_3 = 0.6$.

TABLE VII
PARAMETER INDEX OF VARIOUS SOLUTIONS

Type of solution	λ_1	λ_2	λ_3	o_1	o_2	o_3
I	0.05-0.85	0.12-0.91	0-0.25	1	54.50	49.8512
II	0.02-0.82	0.01-0.57	0.11-0.80	1	66.40	23.3546
III	0.02-0.05	0.87-0.90	0.07-0.09	0.4655	103.24	19.5533

3) Comparison of Transit Models

Finally, the differences between the transit model in [18] and the transit model in this paper are compared. Section III illustrates that the data in the transit time matrix are updated during the iteration process. The update process of the matrix data is shown in Fig. 10, where the rows of the matrix represent the time period and the columns of the matrix represent the transit direction.

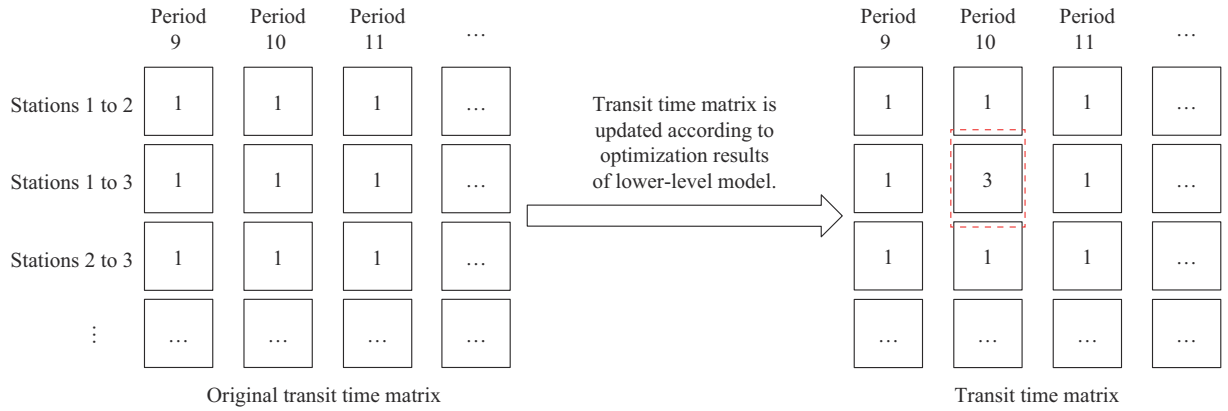

Fig. 10. Update process of transit time matrix.

The original transit time matrix is obtained by performing path planning with the non-stopping strategy. The original transit time matrix ensures the shortest transit time for MESS. Since the lower-level model uses the stopping strategy for route planning, its optimized transit time will be larger than the value in the original transit time matrix. Therefore, the transit time matrix after the data update will not satisfy the consistency condition, and the transit model in [18] may not obtain the optimal solution.

The simulation step is set to be 1 hour considering the speed of solution. The transit time matrix 1 is considered as the original transit time matrix, as shown in Table BV of Supplementary Material B. The transit time matrix 2 is obtained by changing one of the data on the basis of matrix 1, as shown in Table BVI of Supplementary Material B. Substituting matrix 1 into the upper-level model of this paper, the transit scheme of MESS is obtained, as shown in Fig. 11(a). The system profit is \$7219.7, as shown in Table VIII. Substituting matrix 2 into the upper-level model of this paper, the optimized transit scheme of MESS and system profit are unchanged, as shown in Fig. 11(b) and Table VIII, respectively. Substituting matrix 1 and matrix 2 into the transit model in [18], the optimized transit scheme of MESS and system profit are significantly different, as shown in Fig. 11 and Table VIII, respectively. The changes in the transit scheme and system profit confirm the above view that the transit model in [18] is valid only when the transportation network satisfies the consistency condition.

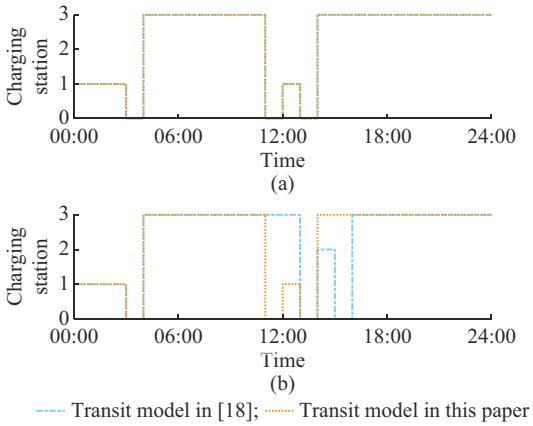

Fig. 11. Comparison of MESS route under different transit models. (a) Transit time matrix 1. (b) Transit time matrix 2.

TABLE VIII
COMPARISON OF DIFFERENT TRANSIT MODELS

Transit model	Transit time matrix	Profit (\$)
Reference [18]	Transit time matrix 1	7219.7
This paper	Transit time matrix 1	7219.7
Reference [18]	Transit time matrix 2	7219.7
This paper	Transit time matrix 2	7136.2

V. CONCLUSION

The increasing number of DGs in the form of RESs in the distribution network provides favorable conditions for the

commercial application of MESS. As a coupling point between power networks and transportation network, the operational scheme of MESS needs to consider the status of both. This paper proposes a bi-level optimal operation model of MESS in coupled transportation-power networks. The upper-level model is an economic scheduling problem for MESS with chance constraints. The lower-level model performs multi-objective fuzzy path planning for MESS based on the optimization result of the upper-level model. Finally, the final optimal operation solution of MESS is obtained by iterative solution of the upper-level and the lower-level models. The verification and analysis of the algorithm show that the optimized operation solution of MESS in this paper avoids the most congestion-prone road sections during each time period, and reduces the energy consumption of MESS during transit while ensuring the stable operation of the distribution network.

REFERENCES

[1] G. Magdy, E. A. Mohamed, G. Shabib *et al*., "Microgrid dynamic security considering high penetration of renewable energy," *Protection and Control of Modern Power Systems*, vol. 3, no. 1, pp. 23-33, Aug. 2018.

[2] K. Ahmed, M. Seyedmahmoudian, S. Mekhilef *et al*., "A review on primary and secondary controls of inverter-interfaced microgrid," *Journal of Modern Power Systems and Clean Energy*, vol. 9, no. 5, pp. 969-985, Sept. 2021.

[3] S. K. Kyung, K. J. McKenzie, Y. L. Liu *et al*., "A study on applications of energy storage for the wind power operation in power systems," in *Proceeding IEEE PES General Meeting*, Montreal, Canada, Jun. 2006, pp. 1-5.

[4] T. Chen, X. Zhang, J. Wang *et al*., "A review on electric vehicle charging infrastructure development in the UK," *Journal of Modern Power Systems and Clean Energy*, vol. 8, no. 2, pp. 193-205, Mar. 2020.

[5] H. Cai, Q. Chen, Z. Guan *et al*., "Day-ahead optimal charging/discharging scheduling for electric vehicles in microgrids," *Protection and Control of Modern Power Systems*, vol. 3, no. 1, pp. 9-33, Apr. 2018.

[6] W. Sun, J. Zhang, J. Yang *et al*., "Probabilistic evaluation and improvement measures of power supply capability considering massive ev integration," *Electronics*, vol. 8, no. 10, pp. 1-18, Oct. 2019.

[7] H. H. Abdeltawab and A. R. I. Mohamed, "Mobile energy storage scheduling and operation in active distribution systems," *IEEE Transactions on Industrial Electronics*, vol. 64, no. 99, pp. 6828-6840, Sept. 2017.

[8] Winston Energy Group Limited. (2021, Jan.). [Online]. Available: http://en.winston-battery.com/index.php/products/mobile-power

[9] EnergyTrend. (2021, Jan.). [Online]. Available: https://www. energytrend.cn/news/20190916-75678.html

[10] EnergyTrend. (2021, Jan.). [Online]. Available: https://www. energytrend.cn/news/20191101-77578.html

[11] Chuneng BJX. (2021, Jan.). [Online]. Available: http://chuneng. bjx.com.cn/news/20201106/1114418.shtml

[12] Chuneng BJX. (2021, Jan.). [Online]. Available: http://chuneng. bjx.com.cn/news/20210104/1126688.shtml

[13] J. Kim and Y. Dvorkin, "Enhancing distribution system resilience with mobile energy storage and microgrids," *IEEE Transactions on Smart Grid*, vol. 10, no. 5, pp. 4996-5006, Sept. 2018.

[14] S. Lei, C. Chen, H. Zhou *et al*., "Routing and scheduling of mobile power sources for distribution system resilience enhancement," *IEEE Transactions on Smart Grid*, vol. 10, no. 5, pp. 5650-5662, Sept. 2019.

[15] S. Yao, P. Wang, and T. Zhao, "Transportable energy storage for more resilient distribution systems with multiple microgrids," *IEEE Transactions on Smart Grid*, vol. 10, no. 3, pp. 3331-3341, Aug. 2019.

[16] S. Yao, P. Wang, and X. Liu, "Rolling optimization of mobile energy storage fleets for resilient service restoration," *IEEE Transactions on Smart Grid*, vol. 11, no. 2, pp. 1030-1043, Jul. 2019.

[17] K. Ling, Z. Guan, H. Wu *et al*., "Active distribution network dispatch strategy with movable storage considering voltage control," *Electric Power Construction*, vol. 38, no. 6, pp. 44-51, Jun. 2017.

[18] S. Y. Kwon, J. Y. Park, and Y. J. Kim, "Optimal operation of mobile energy storage devices to minimize energy loss in a distribution system," in *Proceedings of IEEE International Conference on Environment and Electrical Engineering and IEEE Industrial and Commercial Power Systems Europe*, Palermo, Italy, Jun. 2018, pp. 1-6.

[19] M. E. Baran and F. F. Wu, "Network reconfiguration in distribution systems for loss reduction and load balancing," *IEEE Transactions on Power Delivery*, vol. 4, no. 2, pp. 1401-1407, May 1989.

[20] Y. Liu, W. Wu, B. Zhang *et al*., "A mixed integer second-order cone programming based active and reactive power coordinated multi-period optimization for active distribution network," *Proceedings of the CSEE*, vol. 34, no. 16, pp. 2575-2583, Jun. 2014.

[21] G. He, Q. Chen, C. Kang *et al*., "Optimal bidding strategy of battery storage in power markets considering performance-based regulation and battery cycle life," *IEEE Transactions on Smart Grid*, vol. 7, no. 5, pp. 2359-2367, Sept. 2016.

[22] B. Xu, A. Oudalov, A. Ulbig *et al*., "Modeling of lithium-ion battery degradation for cell life assessment," *IEEE Transactions on Smart Grid*, vol. 9, no. 2, pp. 1131-1140, Mar. 2018.

[23] S. Beak, H. Kim, and Y. Lim, "Multiple-vehicle origin destination matrix estimation from traffic counts using genetic algorithm," *Journal of Transportation Engineering*, vol. 130, no. 3, pp. 339-347, May 2004.

[24] D. E. Kaufman and L. S. Robert. "Fastest paths in time-dependent networks for intelligent vehicle highway systems application," *Journal of Intelligent Transportation Systems*, vol. 1, no. 1, pp. 1-11, Jan. 1993.

[25] J. Lu, Y. Chen, J. K. Chao, "The time-dependent electric vehicle routing problem: model and solution," *Expert Systems with Applications*, vol. 161, pp. 1-17, Dec. 2020.

[26] Y. Zhu, "Modeling technology and optimization method of urban road traffic congestion situation assessment," Ph. D. dissertation, Department of Systems Engineering, Nanjing University of Science and Technology, Nanjing, China, 2018.

[27] B. Ghosh, B. Basu, and M. O'mahony, "Bayesian time-series model for short-term traffic flow forecasting," *Journal of Transportation Engineering*, vol. 133, no. 3, pp. 180-189, Mar. 2007.

[28] M. Castro-Neto, Y. S. Jeong, and M. K. Jeong, "Online-SVR for short-term traffic flow prediction under typical and atypical traffic conditions," *Expert Systems with Applications*, vol. 36, no. 3, pp. 6164-6173, Apr. 2009.

[29] K. Y. Chan, T. S. Dillon, and J. Singh, "Neural-network-based models for short-term traffic flow forecasting using a hybrid exponential smoothing and Levenberg-Marquardt algorithm," *IEEE Transactions on Intelligent Transportation Systems*, vol. 13, no. 2, pp. 644-654, Jun. 2012.

[30] F. Wen, G. Zhang, L. Sun *et al*., "A hybrid temporal association rules mining method for traffic congestion prediction," *Computers & Industrial Engineering*, vol. 130, Apr. 2019.

[31] W. Zhao, X. Sun, S. Si *et al*., "Multi-objective routing optimization of military resources distribution based on fuzzy constraints," *Systems Engineering and Electronics*, vol. 40, no. 12, pp. 2699-2706, Dec. 2018.

[32] Z. Li, W. Wu, J. Zhu *et al*., "Chance-constrained model for day-ahead heat pump scheduling in active distribution network and its tractability transformation," *Automation of Electric Power Systems*, vol. 42, no. 11, pp. 24-31, Jun. 2018.

[33] A. Nemirovski, "On safe tractable approximations of chance constraints," *European Journal of Operational Research*, vol. 219, no. 3, pp. 707-718, Jun. 2012.

[34] M. Jiménez, M. A. Parra, A. Bilbao *et al*., "Linear programming with fuzzy parameters: an interactive method resolution," *European Journal of Operational Research*, vol. 177, no. 3, pp. 1599-1609, Feb. 2007.

[35] L. Zhao and B. Zeng. (2012, Jan.). An exact algorithm for two-stage robust optimization with mixed integer recourse problems. [Online]. Available: http://www. optimizationonline. org/DB_FILE/2012/01/3310. pdf

[36] D. Yury, F. Ricardo, and Y. Wang, "Co-planning of investments in transmission and merchant energy storage," *IEEE Transactions on Power Systems*, vol. 33, no. 1, pp. 245-256, Jan. 2018.

[37] Y. Shao, Y. Mu, X. Yu *et al*., "A spatial-temporal charging load forecast and impact analysis method for distribution network using EVS-traffic-distribution model," *Proceedings of the CSEE*, vol. 37, no. 18, pp. 3-15, Sept. 2017.

[38] M. R. Dorostkar-Ghamsari, M. Fotuhi-Firuzabad, M. Lehtonen *et al*., "Value of distribution network reconfiguration in presence of renewable energy resources," *IEEE Transactions on Power Systems*, vol. 31, no. 3, pp. 1879-1888, May 2016.

[39] M. E. Baran and F. Wu, "Network reconfiguration in distribution systems for loss reduction and load balancing," *IEEE Transactions on*

Power Delivery, vol. 4, no. 2, pp. 1401-1407, Apr. 1989.
[40] S. Lei, Y. Hou, and F. Qiu, "Identification of critical switches for integrating renewable distributed generation by dynamic network reconfiguration," *IEEE Transactions on Sustainable Energy*, vol. 9, no. 1, pp. 420-432, Jan. 2018.
[41] M. Nick, R. Cherkaoui, and M. Paolone, "Optimal siting and sizing of distributed energy storage systems via alternating direction method of multipliers," *International Journal of Electrical Power & Energy Systems*, vol. 72, pp. 33-39, Mar. 2015.
[42] J. Lofberg: "YALMIP: a toolbox for modeling and optimization in MATLAB," in *Proceedings of 2004 IEEE International Symposium on Computer Aided Control Systems Design*, Taipei, China, Jun. 2004, pp. 284-289.
[43] Z. Gu, E. Rothberg, and R. Bixby. (2019, Jan.). Gurobi Optimizer Reference Manual. [Online]. Available: http://www.gurobi.com

Weiqing Sun received the B.Sc., M.Sc., and Ph.D. degrees in electrical engineering from Shanghai Jiao Tong University, Shanghai, China, in 2005, 2009, and 2013, respectively. He is currently a Professor of electrical engineering in University of Shanghai for Science and Technology, Shanghai, China. His research interests include power system planning and optimization, smart grid, demand response, energy storage technology, and artificial intelligence in electrical engineering.

Wei Liu received the B.Sc. degree in electrical engineering from University of Shanghai for Science and Technology, Shanghai, China, in 2019. He is currently pursuing the M.Sc. degree in electrical engineering in University of Shanghai for Science and Technology. His research interests include power system planning and optimization, smart grid, and mobile energy storage technology.

Jie Zhang received the B.Sc. degree in electrical engineering from University of Shanghai for Science and Technology, Shanghai, China, in 2019. She is currently pursuing the M.Sc. degree in electrical engineering in University of Shanghai for Science and Technology. Her research interests include power system planning and optimization, smart grid, and artificial intelligence in electrical engineering.

Kunpeng Tian received the M. Sc. degree in electrical engineering from University of Shanghai for Science and Technology, Shanghai, China, in 2018. He is currently pursuing the Ph.D. degree in control science and engineering in University of Shanghai for Science and Technology. His research interests include power system planning and optimization, ancillary service market, and operation mechanism of load aggregator.